# Supporting Information

Syed et al. 10.1073/pnas.1000309107

## SI Text

**SI Materials and Methods.** ***Preparation of DNA fragments.*** The 423-bp dinucleosomal and 623-bp trinucleosomal DNA fragments (1), containing two and three 601 nucleosome positioning sequences, respectively, were subcloned from the 33x 200–601 chromatin array DNA (kindly provided by Daniela Rhodes, Cambridge, UK). Prior to reconstitution, the fragments were excised from the plasmid either by restriction enzyme EcoRV for cryoEM experiments (611 bp with outer linkers of 36 and 28 bp) or by enzymes XbaI and EcoRI for Klenow radiolabeling. The outer linkers generated were 44 and 32 bp whereas the length of internal linkers was 53 bp in all cases. To determine the cleavage pattern for both strands independently, named upper strand and lower strand for convenience, either strand was separately labeled by fill-in with Klenow at either the EcoRI or XbaI cleaved overhangs, respectively. The 255-bp DNA fragment, containing the 601 nucleosome positioning sequence in the middle, was obtained by PCR amplification from plasmid pGem-3Z-601 (kindly provided by J. Widom, Evanston, IL, and B. Bartholomew, Carbondale, IL) using 5′ labeled primer for the corresponding lower strand of dinucleosome.

***Clone construction and protein purification.*** A clone encoding full-length 227 amino acid residue human H1.5 was used to prepare the deletion mutant peptides 1–177, 1–127, 35–127, 35–120, and 40–112 (GH1) by standard methods. The corresponding proteins were expressed by standard IPTG induction in transformed BL21- RIL bacterial cell line. The soluble proteins were purified first by SP sepharose and then by fractionation over a 1-mL Resource S cation exchange column (Biorad) using FPLC. Mouse NAP-1 (mNAP-1) was also bacterially expressed and purified by Resource Q anion exchange column. Purified proteins were analyzed by 15% SDS-PAGE and stained with Coomassie blue. Recombinant *Xenopus laevis* full-length core histones (H2A, H2B, H3, and H4) were produced in bacteria and purified as described (2).

***Nucleosome reconstitution.*** Mononucleosome, dinucleosome, and trinucleosome particles (without linker histone) were reconstituted by salt dialysis (3). Briefly, chicken erythrocyte carrier DNA fragments (150–200 bp) and 50 ng of $^{32}$P labeled 601 DNA were mixed with equimolar amounts of histone octamer in nucleosome reconstitution buffer (2 M NaCl, 10 mM Tris, pH 7.4, 1 mM EDTA, 5 mM MeEtOH, and 10% glycerol) and serially dialyzed to low salt (10 mM NaCl) buffer. Trinucleosome reconstitutions for cryoEM experiments were carried out without any carrier DNA.

***NAP-1 mediated deposition of H1.*** Full-length H1 or the deletion mutants were mixed with mNAP-1 in a 1:2 molar ratio (buffer 20 mM Tris-HCl, pH 7.5, 0.5 mM EDTA, 100 mM NaCl, 1 mM DTT, 10% glycerol, 0.1 mM PMSF) and incubated at 30 °C for 15 min. Dinucleosomes were mixed with different concentrations of linker histones or linker histone/NAP-1 complexes in binding buffer (15 mM Tris-HCl, 0.3 mM EDTA, 0.2 mM DTT, 2% glycerol, 25 mM NaCl) at 30 °C for 30 min to find the saturation concentrations. Samples were run on 2% agarose gel in 0.3× TBE. After electrophoresis, the gels were dried and analyzed by autoradiography. Dinucleosomes stoichiometrically associated with H1 or deletion mutants were used for DNase I footprinting and analyzed on 8% urea denaturing gel as described previously (4).

***Hydroxyl radical footprinting.*** To perform hydroxyl radical footprinting, samples containing mono-, di-, and trinucleosomes stoichiometrically associated with H1 or deletion mutants were prepared and then exchanged into quencher-free buffer (5 mM Tris, 5 mM NaCl, and 0.25 mM EDTA) by repeated filtration (100 kDa cut-off centricon apparatus). Footprinting was carried out with 15 μL of reaction mixture containing 150 ng of full-length H1- or H1 deletion mutant bound nucleosomes in nucleosomal buffer placed at the bottom of an Eppendorf tube. The hydroxyl radical reaction was initiated by mixing 2.5 μL each of 2 mM $FeAmSO_4$/4 mM EDTA, 0.1 M ascorbate, and 0.12% $H_2O_2$ together in a drop on the side of the reaction tube before mixing rapidly with the reaction solution. The concentration of Fe (II)EDTA in the reaction mixture was varied to achieve different cleavage yields. The reaction was terminated by addition of 100 μL stop solution (0.1% SDS, 25 mM EDTA, 1% glycerol, and 100 mM Tris, pH 7.4), and the DNA was purified by phenol/chloroform extraction and ethanol/glycogen precipitation. Raw intensity traces of •OH footprinting gels were processed by automated band counting, bandwise integration, and finally rescaling within a moving window (see Fig. S4). The resulting signal represents the relative •OH accessibility per nucleotide, corrected for global trends and for irregularities in the gel. The data are quantitative for the location and phasing of protected sites but provide only qualitative information on the degree of protection.

***Cryoelectron microscopy.*** Trinucleosome reconstitutions were performed without any carrier DNA. Full-length H1 and H1 deletion mutants were deposited in complex with mNAP-1 as described above. The final reaction mixes were concentrated to 200 ng/μL of DNA and the buffer exchanged to nucleosomal buffer using 100 kDa cut-off centricons. Immediately after the buffer exchange, the samples were prepared for cryoelectron microscopy as described earlier (5). Briefly, a 3-μL droplet of the solution was deposited on an electron microscopy grid with a homemade perforated supporting film with the surface treated by successive evaporation of carbon and platinum/carbon layers. The excess of the solution was removed by brief blotting using Whatman no. 1 filter paper and the grid immediately plunged into liquid ethane (−183 °C). The grid was transferred without rewarming into a Tecnai G2 Sphera 20 electron microscope using a Gatan 626 cryotransfer holder. The sample was visualized at 80 kV acceleration potential using low dose operation mode with total electron dose not exceeding 15 e/s$Å^2$. Images were recorded on a Gatan Ultrascan1000 slow scan CCD camera at microscope nominal magnification either 14,500× or 25,000× (final pixel size 0.7 and 0.4 nm) with 2.5 μm underfocus.

***Structural model rebuilding.*** We built a three-DNA binding site model by manually matching the GH1 α-helix orientations and the •OH footprint-derived DNA protected sites. We have used a very similar orientation to that described for GH5 with the corresponding contacting residues in the resulting structure as proposed by Fan and Roberts (6). The positively charged chains of GH5, which contact nucleosomal DNA, were found to be conserved among the other linker histones, thus indicating that this mode of interaction would be also applicable for the globular domains of the other linker histones (6). Remarkably, this GH1 structure (7) was large enough to fill the space between the entering and exiting linker DNA and to precisely interact with protected sites in both linkers and the nucleosome dyad (Fig. 6*B*,

Fig. S5*A*, and Movie S2). Therefore in this three-contact GH1-nucleosome model, in contrast to the GH5 binding model of Fan and Roberts (6), no bending of the linker DNA is required.

Two alternative two-contact models were considered. Zhou et al. proposed an arrangement of the linker histone (8) based on cross-linking experiments with mutated GH5. Brown et al. proposed a rigid docking refinement (9) of a molecular model for H1 placement between core DNA and one somewhat bent linker. We rebuilt both conformations by deforming one of the linkers in the DNA model and manually matching the location and helix orientations of the docking solution respectively shown in refs. 8 (Fig. S5*B*) and 9 (Fig. S5*C*). We used the same molecular model (1ghc, conformer 8) for the H1 globular domain as for the three-contact model, whose shape gives close-fitting molecular contacts also into the two-contact positions. Note that the structure being symmetric, the model should be interpreted as one of two coexisting configurations, each with one linker contacted.

***Coarse-grained modeling at the base-pair level.*** We have carried out a restrained energy minimization with the boundary conditions of free linker ends and linker start base pairs fixed in their nucleosome core particle conformation (10). For energy minimization, we have employed the sequence-dependent rigid base-pair model of DNA elasticity (with the "MP" parameter set, as described in refs. 11 and 12). DNA volume exclusion was included by placing purely repulsive Lennard–Jones spheres with 2.05 nm diameter around each base pair. To enforce contacts between the two DNA linkers at the corresponding maximally protected sites, linear springs were introduced between the C5′ atom positions at the minima of the full-H1 accessibility profile. As a final step, we used the 3DNA- software to reintroduce atomic details into the coarse-grain structures (13).

***Visualization.*** The molecular visualization package Chimera (14) allows rendering of molecular structures using a color code for user-defined atom attributes. This feature was used to present the relative accessibility signals from the footprinting experiments by color coding the deoxyribose C5′ atoms. Footprints were measured for one of the strands. Color coding on both strands of DNA was displayed, by exploiting the twofold symmetry of the nucleosome. Bases for which no single nucleotide resolution footprinting was available were not colored.

***Structure-derived accessibility profiles.*** DNA is attacked by •OH radicals primarily at the C5′ atoms of the backbone sugars, and •OH attack efficiency is determined by the accessible surface area at these sites. Per-C5′ unified atom accessible surfaces were calculated with the MSMS program (15) as implemented in Chimera (14). Lacking the resolution of single protons in our structural models, we somewhat simplified the procedure from ref. 16, considering solvent accessible surface areas of C5′ atoms directly and using "unified van der Waals radii" (17) to account implicitly for the hydrogens. To mimic the smoothing effect of thermal fluctuations, we increased the probe radius to 3 Å. After a moving average over the resulting trace with a 3-bp window, predicted accessibility patterns for both strands in each complex were averaged to account for the strand-exchange symmetry observed in experimental footprints (Fig. S5*D*).


1. Syed SH, et al. (2009) The incorporation of the novel histone variant H2AL2 confers unusual structural and functional properties of the nucleosome. *Nucleic Acids Res* 37(14):4684–4695.
2. Luger K, Rechsteiner TJ, Richmond TJ (1999) Expression and purification of recombinant histones and nucleosome reconstitution. *Methods Mol Biol* 119:1–16.
3. Mutskov V, et al. (1998) Persistent interactions of core histone tails with nucleosomal DNA following acetylation and transcription factor binding. *Mol Cell Biol* 18:6293–6304.
4. Angelov D, et al. (2003) The histone variant macroH2A interferes with transcription factor binding and SWI/SNF nucleosome remodeling. *Mol Cell* 11:1033–1041.
5. Doyen CM, et al. (2006) Dissection of the unusual structural and functional properties of the variant H2A.Bbd nucleosome. *EMBO J* 25(18):4234–4244.
6. Fan L, Roberts VA (2006) Complex of linker histone H5 with the nucleosome and its implications for chromatin packing. *Proc Natl Acad Sci USA* 103(22):8384–8389.
7. Cerf C, et al. (1994) Homo- and heteronuclear two-dimensional NMR studies of the globular domain of histone H1: Full assignment, tertiary structure, and comparison with the globular domain of histone H5. *Biochemistry* 33(37):11079–11086.
8. Zhou YB, Gerchman SE, Ramakrishnan V, Travers A, Muyldermans S (1998) Position and orientation of the globular domain of linker histone H5 on the nucleosome. *Nature* 395(6700):402–405.
9. Brown DT, Izard T, Misteli T (2006) Mapping the interaction surface of linker histone H1(0) with the nucleosome of native chromatin in vivo. *Nat Struct Mol Biol* 13(3): 250–255.
10. Luger K, Mäder AW, Richmond RK, Sargent DF, Richmond TJ (1997) Crystal structure of the nucleosome core particle at 2.8 A resolution. *Nature* 389:251–260.
11. Becker NB, Everaers R (2007) From rigid base pairs to semiflexible polymers: coarse-graining DNA. *Phys Rev E* 76(2 Pt 1):021923.
12. Becker NB, Wolff L, Everaers R (2006) Indirect readout: Detection of optimized subsequences and calculation of relative binding affinities using different DNA elastic potentials. *Nucleic Acids Res* 34(19):5638–5649.
13. Lu XJ, Olson WK (2003) 3DNA: A software package for the analysis, rebuilding and visualization of three-dimensional nucleic acid structures. *Nucleic Acids Res* 31(17):5108–5121.
14. Pettersen EF, et al. (2004) UCSF Chimera—A visualization system for exploratory research and analysis. *J Comput Chem* 25(13):1605–1612.
15. Sanner MF, Olson AJ, Spehner JC (1996) Reduced surface: an efficient way to compute molecular surfaces. *Biopolymers* 38(3):305–320.
16. Pastor N, Weinstein H, Jamison E, Brenowitz M (2000) A detailed interpretation of OH radical footprints in a TBP-DNA complex reveals the role of dynamics in the mechanism of sequence-specific binding. *J Mol Biol* 304(1):55–68.
17. Tsai J, Taylor R, Chothia C, Gerstein M (1999) The packing density in proteins: standard radii and volumes. *J Mol Biol* 290(1):253–266.

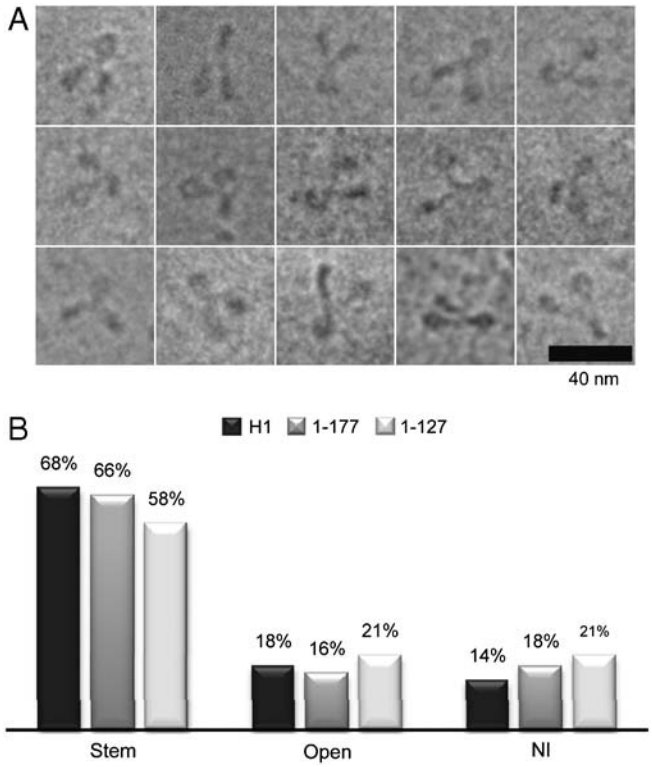


**Fig. S1.** (*A*) Representative electron cryomicroscopy images of reconstituted 601 trinucleosomes assembled with histone H1 truncated mutant 1–177 (in this mutant the last 50 aa from the H1 COOH terminus were removed). (Scale bar, 40 nm.) (*B*) Quantification of the stem structure of the central nucleosome within trinucleosomes reconstituted with either full-length H1 or its truncated mutants 1–127 and 1–177. For statistical analysis, images of 345 trinucleosomes with the full-length H1, 379 trinucleosomes with the truncated mutant 1–127, and 163 trinucleosomes with the mutant 1–177 were used. Stem, stem structure of the central nucleosome; open, open structure of the central nucleosome; NI, nonidentified (the spatial orientation of the trimers did not allow the unambiguous determination of a stem or open structure).

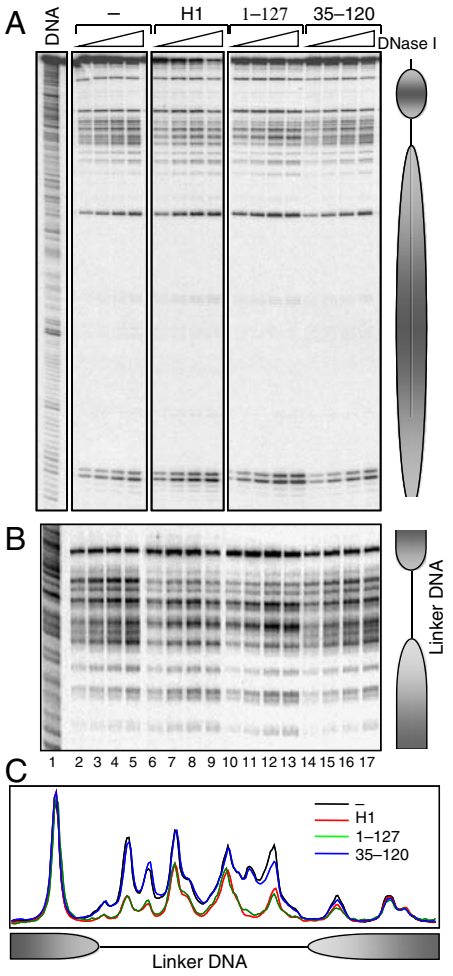


**Fig. S2.** DNase I footprinting of 601 dinucleosomes containing either full-length histone H1 or the truncated mutants 1–127 or 35–120. (*A*) NAP-1 was used to assemble dinucleosomes with either H1 or its truncated mutants, the samples were digested with DNase I, and DNA was isolated from the digested samples and run on an 8% PAGE under denaturing conditions. A schematic drawing of the dinucleosome is shown in the right part of the figure. DNA, DNase I digestion pattern of naked DNA. (*B*) DNase I footprinting of the linker DNA of the different dinucleosome samples. The part of *A* that corresponds to the footprinting of the linker was presented in an enlarged form to visualize better the differences in the DNase I digestion pattern. In the lower panel are shown the scans of lanes 5, 9, 13, and 17 corresponding to the DNase I digestion patterns of control (-), H1, and the mutants 35–120 and 1–127, respectively. The positions of the nucleosomes and the linker DNA are indicated in each panel.

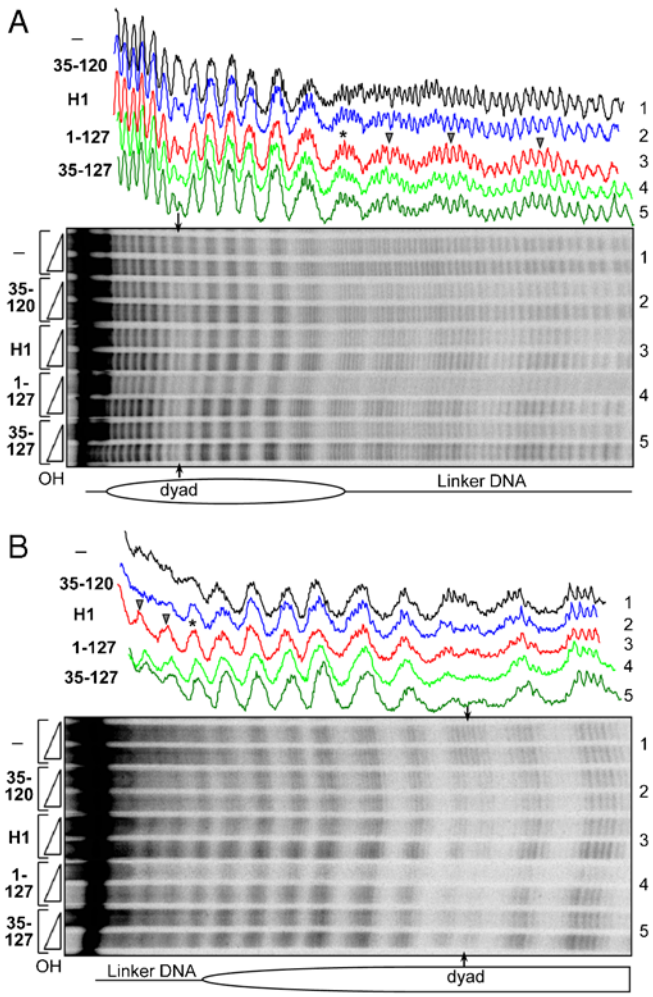


**Fig. S3.** Hydroxyl radical footprinting of mononucleosomes containing NAP-1 incorporated either full-length histone H1 or the indicated histone H1 truncated mutants. Centrally positioned mononucleosomes were reconstituted on $^{32}$P-end labeled 255 bp 601 DNA sequence, and NAP-1 was used to deposit either full-length histone H1 or the indicated H1 mutants. The samples were then treated with OH°, and DNA was purified from the digested samples and run on 8% denaturing PAGE. The electrophoresis was carried out for either less migrated products (*A*) or more migrated products (*B*). In the upper part of each panel are shown the scans of the OH° cleavage patterns of the respective samples. The numbers of the first and the last amino acid residue of the truncated mutants are indicated. (-) control mononucleosomes; (▼) cleavage products corresponding to the central part of the linker DNA; (*) cleavage products corresponding to a DNA fragment at the end of the linker DNA; (↓) designates the footprinting at the nucleosome dyad. In the lower part of each panel a schematic drawing of the mononucleosome is shown. The position of the dyad of the nucleosome as well as this of linker DNA is indicated. Note the structuring of the linker DNA in the mononucleosomes assembled with full-length H1 or with either 35–127 or 1–127 H1 truncated mutants. In contrast to these samples, only one 10-bp linker DNA repeat (designated by *) is observed for the nucleosome assembled with the 35–120 mutant. All the samples assembled with either one of the different H1 truncated mutants, but not the control sample (without H1), show a clear footprinting at the nucleosome dyad.

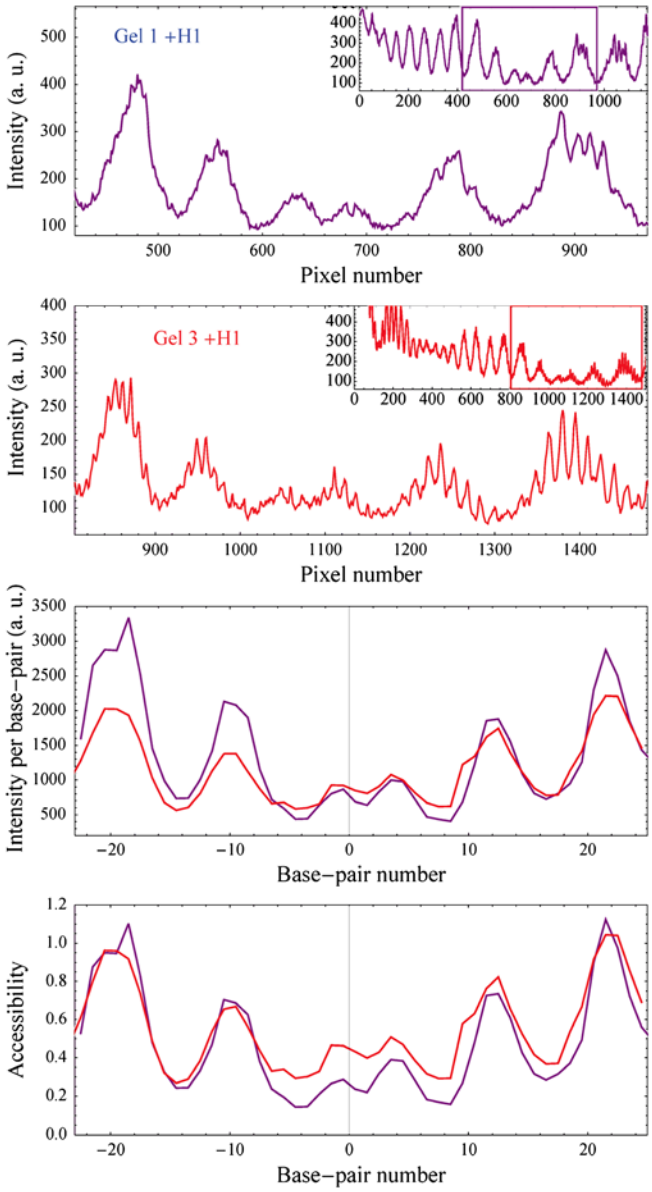


**Fig. S4.** Processing steps of the footprinting signal in presence of H1. For comparison, independent signals from a mononucleosome (*Purple*) and a dinucleosome (*Red*) in the same region (50 bp around the dyad) are shown. From top to bottom: Raw intensities of both gels (*Inset*: complete signal and processing window), superposed intensities per base pair, and relative accessibilities.

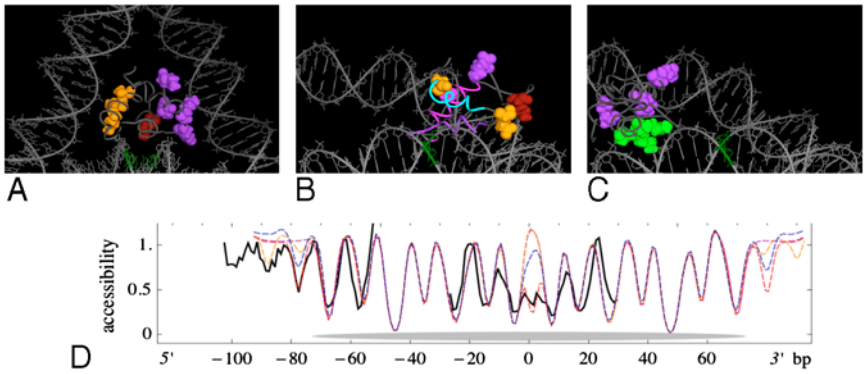


**Fig. S5.** Structural models comparison. (*A*) Three-contact nucleosome configuration. The contacting residues are Lys47, Lys51, and Ser52 (site I, *Orange*); Lys63 (site II, *Red*); and Lys18, Arg20, Arg72, and the C terminal Arg75 (site III, *Purple*). They correspond to the contacts proposed in ref. 6. The viewing direction is the superhelical axis, but rotated by around the dyad axis. (*B*) Two-contact nucleosome configuration. Contact is established with core DNA at 1–4 bp from the dyad, and with one DNA linker (the other linker is not shown). The GH1 -helices I (*Cyan*), II (*Purple*), and III (*Magenta*) are colored as in ref. 8; the C terminal Lys75 is shown in purple, Lys63 is shown in red, contacting linker DNA. The residues Ser7, 19, and 49 mutated as in ref. 8 are shown in orange. The viewing direction is the superhelical axis. (*C*) Two-contact nucleosome configuration. Residues contacting core DNA about 5 bp away from the dyad are Lys47, Lys51, and Ser52 and are colored light green; residues contacting one DNA linker are Arg20, Arg72, and Lys75 (leftmost) and are colored purple. These contacts correspond to those in ref. 9. The viewing direction is the superhelical axis. (*D*) Structure-derived relative accessibility for mononucleosomes with globular H1, based on pure mononucleosome (*Magenta*) and on the GH1 placement models: two-contact B (*Blue*) and C (*Orange*) and three-contact (*Red*). The predictions differ in the protection at the dyad where the two-contact models show no or very weak protection and at the entry/exit linkers. The measured relative accessibility for GH1 is shown in black.

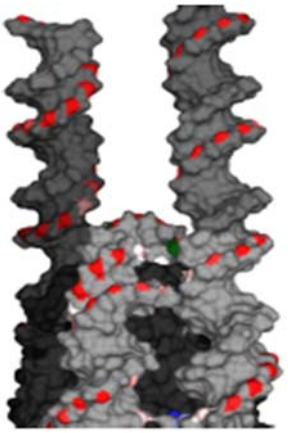

**Movie S1.** Nucleosome without histone H1.
Movie S1 (MOV)

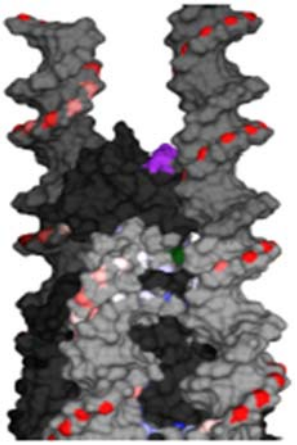

**Movie S2.** Three-contact model for a nucleosome associated with the globular domain (GH1) of histone H1.
Movie S2 (MOV)

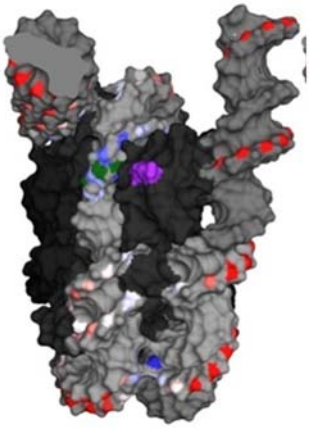

**Movie S3.** Two-contact model (8) of a nucleosome with the globular domain (GH1) of histone H1.
Movie S3 (MOV)

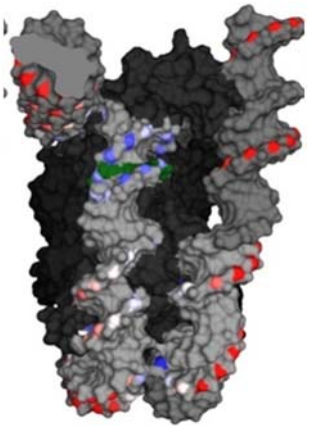

**Movie S4.** Two-contact model (9) of a nucleosome with the globular domain (GH1) of histone H1.
Movie S4 (MOV)

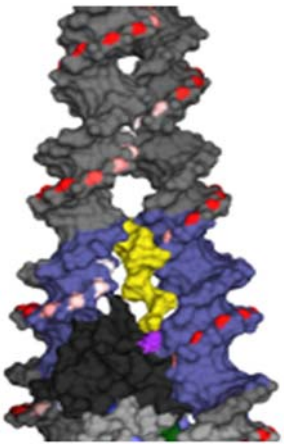

**Movie S5.** Three-contact model for a nucleosome associated with the 40–127 mutant of histone H1.
Movie S5 (MOV)